High-Resolution Reconstruction of Arterial Spin Labelling MRI Using Anatomical Priors

Abolfazl Mehranian[1], Enrico De Vita[1], Radhouene Neji[1,3], Colm J. McGinnity[2], Alexander Hammers[2] and Andrew J. Reader[1]
School of Biomedical Engineering and Imaging Sciences, King's College London, [1]Department of Biomedical Engineering and [2]King's College London & Guy's and St Thomas' PET Centre, St. Thomas' Hospital, London, UK, [3]MR Research Collaborations, Siemens Healthcare Limited, Frimley, UK

***Abstract*—**This work investigates super-resolution reconstruction and deconvolution of perfusion arterial spin labelling (ASL) images using a high-resolution T1-weighted MRI with the aim of reducing the partial volume effect on the estimated cerebral blood flow (CBF). The MR acquisition matrix was factorized to model the down-sampling and blurring of the underlying ASL images, as well as MR coil sensitivity, Fourier encoding and k-space undersampling. The proposed methods were evaluated using simulation and real data in comparison with the standard reconstruction method, and an anatomical non-local means filtering combined with deconvolution. In simulations, both MR-guided deconvolution and reconstruction methods achieved the lowest normalised root mean square (NRMS) errors of 20% and 18.5% respectively, compared to the standard method with NRMS error of 29.5%. For real data, the guided deconvolution gave rise to the best results in terms of contrast and detail recovery. Evaluation of the guided reconstruction of the real data is in progress. In conclusion, the proposed methods provide a promising solution for improving the quality and quantitative accuracy of estimated CBF maps.

***Keywords*—** Arterial spin labelling, perfusion MRI, partial volume correction.

I. Introduction

Arterial spin labelling (ASL) is a perfusion-weighted magnetic resonance imaging (MRI) technique for absolute quantification of cerebral blood flow (CBF). In this technique, the blood water flowing into the brain is magnetically labelled and a perfusion signal is obtained from the subtraction of the acquired label image from a control image with no labelling [1]. Since ASL imaging exploits magnetically labelled blood water as an endogenous tracer, it is totally non-invasive and it can be utilized in repetitive follow-ups; it can therefore substitute other perfusion imaging techniques that rely on an exogenous tracer such as dynamic susceptibility contrast (DSC) MRI or emission tomography with their associated risks. ASL can be acquired with spin echo sequences which are robust to susceptibility signal loss compared to gradient echo based DSC MRI. In addition, ASL has better temporal and spatial resolution than emission tomography modalities such as PET and SPECT.

Nonetheless, all these advantages are challenged by the intrinsically low signal to noise ratio (SNR) of the ASL signal, since the volume of the labelled blood is only about 1% of the total cerebral blood volume. In order to improve SNR and acquire a perfusion image in a clinically acceptable time frame, typically 10–50 control-label image pairs with low resolutions (in-plane: 3–4 mm, through-plane: 4–8 mm) are acquired [2]. This coarse spatial resolution results in partial volume effect (PVE) in the CBF maps leading to significant underestimation of CBF in the grey matter [3]. Furthermore, similar to emission tomography, the point spread function (PSF) of the MR scan can contribute to PVE. For instance, in 3D GRASE, which is a widely used ASL readout sequence, the T2 decay of the echo train signal results in blurring in the partition (through-plane) direction of the imaging volume. In a single-shot GRASE, the through-plane PSF has been reported in the range of 1.5 to 1.9 voxels full width at half maximum (FWHM) [4]. For partial volume correction (PVC), existing methods mainly aim to correct for the tissue fraction effect (caused by low-resolution acquisitions) using partial volume (PV) estimates that are obtained from anatomical MR images mapped into the ASL image resolution. These methods are linear regression [5], modified least trimmed squares [3] or Bayesian inference [6] among others. PV estimation requires accurate segmentation and down-sampling of the anatomical MR images, which are prone to bias errors [7]. These PVC methods can be preceded by a deconvolution pre-processing step to remove the PSF blurring [8] however, the employed deconvolution steps are known to amplify noise and to induce Gibbs ringing artefacts. Another, more direct, way to avoid PVEs is to increase the resolution in the ASL images using smaller voxel sizes, and increase the number of averages to compensate for reduced SNR. However, this would lead to impractically long scan times and increased sensitivity to motion artefacts.

In this work, we propose to perform i) super-resolution reconstruction of control-label image pairs from k-space data and ii) super-resolution deconvolution of the standard CBF maps (obtained from the subtraction of low-resolution control and labelled images), both using high-resolution anatomical MR images. These techniques should allow enhancement of the spatial resolution of the ASL images and hence reduce PVE in the estimated CBF maps.

II. Material and Methods

A. High-resolution reconstruction of ASL data

In the Bayesian framework, the reconstruction of low-resolution ASL data at the high resolution of anatomical MR images can be achieved by the following minimization:

$$\hat{\boldsymbol{x}}^{(i)} = \underset{\boldsymbol{x}^{(i)}\in\mathbb{C}^N}{\operatorname{argmin}} \left\{ \frac{1}{2} \left\| \boldsymbol{\Phi F C H B x}^{(i)} - \boldsymbol{s}^{(i)} \right\|_{\boldsymbol{W}}^{2} + \frac{\beta}{2} \left\| \boldsymbol{D x}^{(i)} \right\|_{\boldsymbol{\omega}}^{2} \right\} \qquad (1)$$

where $i \in \{c, l\}$ indicates control and label datasets, $\boldsymbol{x}$ is the underlying high-resolution image, $\boldsymbol{B}$ is the MR scan blurring matrix, $\boldsymbol{H}$ is the down-sampling matrix from the anatomical image space to ASL space, $\boldsymbol{C}$ is the MR coil sensitivity matrix, $\boldsymbol{F}$ is the Fourier encoding matrix, $\boldsymbol{\Phi}$ is the k-space undersampling matrix, $\boldsymbol{s}$ is the MR measured data, $\boldsymbol{W}$ is the inverse of the noise-correlation matrix, $\boldsymbol{D}$ is a derivative matrix for calculation of local differences between image voxels, $\boldsymbol{\omega}$ is a diagonal matrix used to weight the local differences of image $\boldsymbol{x}$ based on their proximity and similarity in a prior anatomical MR image and β controls the strength of the regularization term. Therefore, the minimization in (1) seeks to reconstruct a high resolution image from low-resolution k-space data with the guidance of a prior high-resolution MR image.

B. High-resolution deconvolution of CBF maps

Under certain conditions, it can be shown that the k-space reconstruction in (1) degenerates to image-space deblurring of the inverse Fourier transform of k-space data. This motivates investigation of super-resolution deblurring as a post-processing step to estimate high-resolution perfusion or CBF maps, $\boldsymbol{x}^{(h)}$, from a low-resolution PVE affected one, $\boldsymbol{x}^{(l)}$, using the following minimization:

$$\hat{\boldsymbol{x}}^{(h)} = \underset{\boldsymbol{x}^{(h)}\in\mathbb{C}^N}{\operatorname{argmin}} \left\{ \frac{1}{2} \left\| \boldsymbol{H B x}^{(h)} - \boldsymbol{x}^{(l)} \right\|_{2}^{2} + \frac{\beta}{2} \left\| \boldsymbol{D x}^{(h)} \right\|_{\boldsymbol{\omega}}^{2} \right\} \qquad (2)$$

In this study, we used Gaussian similarity kernels, with an additional parameter, σ, to calculate the weighting coefficients $\boldsymbol{\omega}$ in Eqs. (1-2), similar to [9]. The minimizations in Eqs. (1-2) were solved iteratively using the conjugate gradient (CG) algorithm [10].

C. Simulations and real data

For realistic simulations, the structural T1-weighted image of a volunteer (with resolution of 1.05×1.05×1.1 mm^3) was segmented into grey matter (GM) and white matter (WM), and an equilibrium magnetisation (M0) and a ground truth CBF map were simulated. Based on reported healthy human CBF values [11], the values of 65 and 20 mL/100g/min were assigned to GM and WM voxels, respectively. Regions of cortical hyper-perfusion and hypo-perfusion (on average 78 and 10 mL/100g/min, respectively) were also artificially created. The control image was assumed to be the M0 image and the label image was calculated in each voxel by using a single-compartment perfusion model [12]. The control-label image pairs were smoothed using an anisotropic Gaussian kernel (4,4,8) mm FWHM and down-sampled to the resolution of 3.52×3.53×5.06 mm^3. Noisy multi-channel k-space data (5 channels) were generated from the resulting low-resolution control-label image pairs. For performance comparisons, a k-space undersampling factor of 4 was considered. An ASL dataset was acquired for a healthy volunteer with the following parameters: pseudo-continuous ASL (PCASL) labelling (labelling duration 1.5s, post-labelling delay 1.8s) and 3D GRASE readout [13], EPI factor of 31, 26 slices with oversampling of 10%, slice thickness 4 mm, in-plane resolution of 4×4 mm^2, 21 control-label measurements together with one proton density weighted (M0) images were acquired within a total scan time of 6 minutes. Additionally, a T1 weighted image was acquired using a 3D magnetization prepared rapid gradient echo (MPRAGE) sequence.

D. Evaluation metrics

The performance of the proposed MR-guided super-resolution reconstruction and deconvolution methods were compared with the standard perfusion image (obtained from the subtraction of the control and label pairs), the perfusion image filtered with different methods such as PSF deconvolution, anatomical non-local means (A-NLM) filtering [14] and combined A-NLM and deconvolution. For the simulations, the GM and WM quantification errors were evaluated with respect to the ground truth perfusion maps as follows:

$$E_i = 100 \times \frac{x_i - x_i^{Truth}}{x_i^{Truth}} \qquad (3)$$

In addition, the normalized root mean square error (NRMSE) in the whole brain was calculated as:

$$NRMSE = 100 \times \sqrt{\frac{\sum_i \left| x_i - x_i^{Truth} \right|^2}{\sum_i \left| x_i^{Truth} \right|^2}} \qquad (4)$$

The real data results were evaluated in terms of mean GM CBF in different tissue fraction ranges.

III. Results

A. Simulations

Fig. 1 shows the simulation results for different methods including i) the low-resolution standard method, ii) the deconvolution of the standard image, up-sampled into the resolution of the T1-MPRAGE image, using a PSF kernel of (4,4,7) mm in FWHM, iii) A-NLM filtering of the up-sampled standard image, iv) deconvolution of the A-NLM image, v-vi) T1-guided deconvolution and reconstruction methods. The quantitative performance of the methods is also shown using voxel-wise error maps. As shown the standard reconstruction methods suffers from noise and loss of structural information due to PVEs. The deconvolution, performed using 30 iterations of the CG algorithm, enhances the overall contrast, particularly in striatum, however at the expense of amplifying noise. The A-NLM filtering in which the Gaussian similarity coefficients were derived from the high-resolution T1 image reduces noise

but suffers from PVE and low-contrast resolution. Deconvolution of the A-NLM image (30 iterations of the CG algorithm) results in notable improvements in terms of contrast, quantification errors (see Fig. 2A-B) at the cost of increased Gibbs artefacts at the borders. As shown, both high-resolution guided deconvolution and reconstruction methods give rise to noise reduction, higher contrast-resolution and recovery of tissue-type boundaries. For these simulated data reconstructions, the regularization used $\sigma = 0.2$ and β was chosen based on minimal NRMSE in the whole brain. Fig. 2A-B shows the mean and standard deviation of the quantification errors in GM and WM as well as the NRMSE in the whole brain. The results show that the guided reconstruction method achieves the best performance. In GM, it reduces the errors of the standard method from –14±71% to –4±63%, while in WM, the errors are reduced from +21±38% to +12±25%. The whole brain NRMSE is reduced from 29.5% to 20% and 18.5%, respectively for the proposed guided deconvolution and reconstruction. Fig. 2 C-D shows profiles through the simulated hyper-perfused region, which is subject to substantial PVEs as seen in the standard reconstruction method. The profiles demonstrate that the proposed methods, particularly the guided reconstruction method, result in improved recovery of the true intensity profiles.

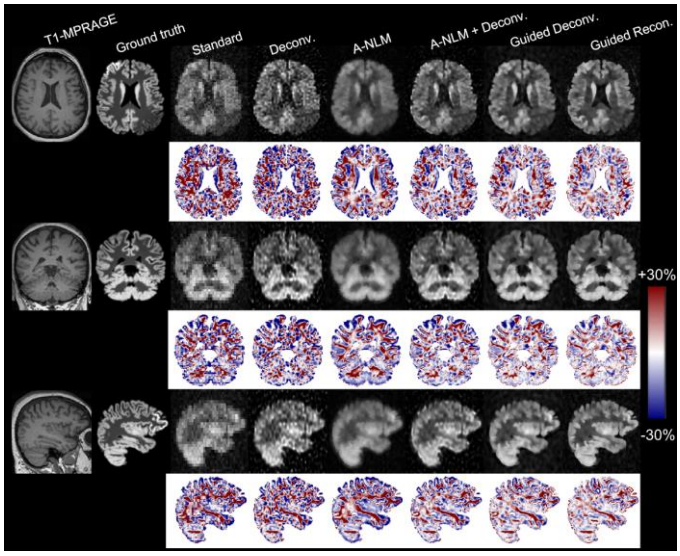

Fig. 1. Reconstruction results of simulated ASL data with k-space undersampling factor of 4. Left to right: high-resolution T1-MPRAGE and ground truth perfusion images (1.05×1.05×1.1 mm^3), low-resolution standard reconstruction (3.52×3.53×5.06 mm^3), PSF deconvolution of standard reconstruction up-sampled to T1 image resolution, anatomical non-local means (A-NLM) filtering of the up-sampled standard image, deconvolution of the A-NLM image, the proposed high-resolution guided deconvolution and reconstructions. The voxel-wise error maps have also been shown.

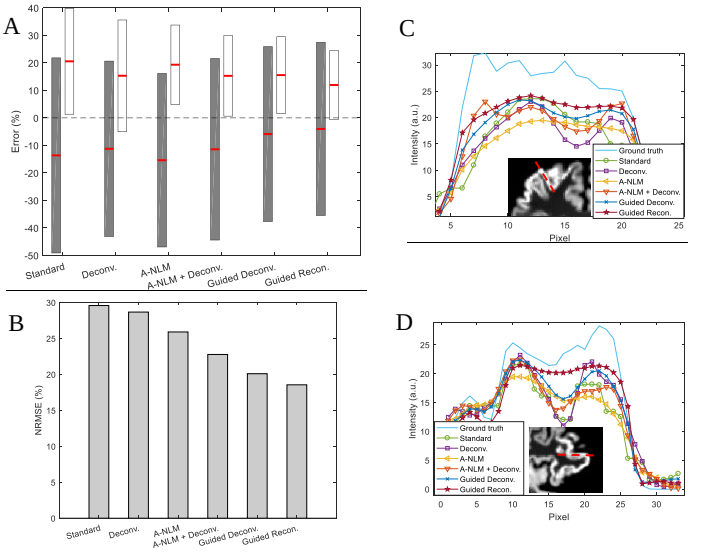

Fig. 2. A) Mean (horizontal red mark) and standard deviation (vertical bar) of the errors in grey (grey) and white matter (white) for the different methods. B) NRMSE over the whole brain for the different methods. C-D) Intensity profiles through the dashed lines indicated in the inset (showing ground truth for hyper-perfused regions) in transverse and sagittal views.

B. Real data

For real data, in this preliminary work, we evaluated the different post-reconstruction methods on the control-label image pairs as reconstructed by the scanner. Indeed clinical scanners typically produce only magnitude images. The guided reconstruction of complex k-space data will be addressed in the near future. The image pairs were averaged over the 21 measurements and converted into CBF maps using the FSL software (FMRIB, Oxford, UK). The low-resolution standard CBF maps were then processed using different methods as shown in Fig. 4. Similar to the simulations, the deconvolution method was performed on the up-sampled CBF image

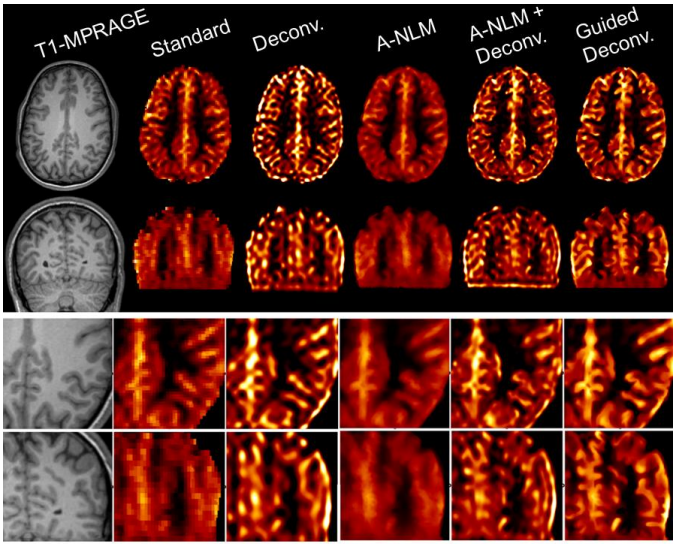

Fig. 3. Comparison of different post-processing methods operating on the low-resolution standard CBF map.

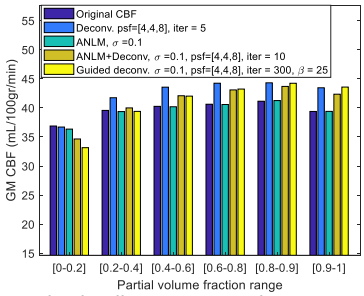

Fig. 4. Grey matter cerebral blood flow for different partial volume fraction ranges obtained from the segmented image of the T1-weighted MR image of the healthy volunteer.

using the CG algorithm for only 5 iterations (further iterations resulted in extensive Gibbs artefacts) and PSF widths of (4,4,8) mm FWHM. The A-NLM method shows some edge enhancement but lacks contrast. The deconvolution of the A-NLM image leads to contrast recovery however at expense of increased Gibbs artefacts. As can be seen, the guided deconvolution method gives rise to improved noise reduction, contrast recovery and enhanced tissue boundaries. The regularization parameter was selected experimentally to give best grey-white matter contrast with reduced artefacts. The PVC performance of the methods was evaluated based on the mean CBF in different PV (or tissue) fractions of grey matter. A PV (grey matter probability) map was obtained from the segmentation of the T1-weighted MR image using the SPM software (Wellcome Trust Centre for Neuroimaging, UCL). The results show that for PV fraction [0-0.2] the guided deconvolution results in the lowest CBF value, which is due to reduced spill-out of GM in WM by these methods. For higher ranges of PV fraction, the proposed method results in increased GM CBF. The conventional deconvolution methods also result in higher CBF values, however, this can be attributed to the increased Gibbs artefacts at the edges.

IV. Conclusion

In this work, advanced MR-guided super-resolution methods were proposed to reduce PVEs in ASL images and hence to improve the quantitative accuracy of the estimated CBF maps. The results show that the super resolution modelling and reconstruction or processing of the ASL images in the high-resolution space of the anatomical T1-weighted images can improve the quality and quantitative accuracy of the CBF maps. Future work will include guided reconstruction of the complex real data and comparison of the proposed methods with the standard PVC techniques currently in use.

References

[1] J. A. Detre, J. S. Leigh, D. S. Williams, and A. P. Koretsky, "Perfusion imaging," *Magn. Reson. Med.*, vol. 23, no. 1, pp. 37–45, 1992.

[2] D. C. Alsop *et al.*, "Recommended implementation of arterial spin-labeled perfusion MRI for clinical applications: A consensus of the ISMRM perfusion study group and the European consortium for ASL in dementia," *Magn. Reson. Med.*, vol. 73, no. 1, 2015.

[3] X. Liang, A. Connelly, and F. Calamante, "Improved partial volume correction for single inversion time arterial spin labeling data," *Magn. Reson. Med.*, vol. 69, no. 2, pp. 531–537, 2013.

[4] M. A. Fernández-Seara *et al.*, "Continuous arterial spin labeling perfusion measurements using single shot 3D GRASE at 3 T," *Magn. Reson. Med.*, vol. 54, no. 5, pp. 1241–1247, 2005.

[5] I. Asllani, A. Borogovac, and T. R. Brown, "Regression algorithm correcting for partial volume effects in arterial spin labeling MRI," *Magn. Reson. Med.*, vol. 60, no. 6, pp. 1362–1371, 2008.

[6] M. A. Chappell, A. R. Groves, B. J. MacIntosh, M. J. Donahue, P. Jezzard, and M. W. Woolrich, "Partial volume correction of multiple inversion time arterial spin labeling MRI data," *Magn. Reson. Med.*, vol. 65, no. 4, pp. 1173–1183, 2011.

[7] A. Fazlollahi *et al.*, "Reproducibility of multiphase pseudo-continuous arterial spin labeling and the effect of post-processing analysis methods," *Neuroimage*, vol. 117, pp. 191–201, 2015.

[8] I. B. Galazzo, M. A. Chappell, D. L. Thomas, X. Golay, P. Manganotti, and E. De Vita, "Reducing blurring artifacts in 3D-GRASE ASL by integrating new acquisition and analysis strategies," in *Proc. Intl. Soc. Mag. Reson. Med*, 2014, p. 2704.

[9] A. Mehranian *et al.*, "PET image reconstruction using multi-parametric anato-functional priors," *Phys. Med. Biol.*, vol. 62, no. 15, p. 5975, 2017.

[10] K. P. Pruessmann, M. Weiger, P. Börnert, and P. Boesiger, "Advances in sensitivity encoding with arbitrary k-space trajectories," *Magn. Reson. Med.*, vol. 46, no. 4, pp. 638–651, Oct. 2001.

[11] K. Zhang *et al.*, "Comparison of cerebral blood flow acquired by simultaneous [15O]water positron emission tomography and arterial spin labeling magnetic resonance imaging.," *J. Cereb. Blood Flow Metab.*, vol. 34, no. 8, pp. 1373–1380, Aug. 2014.

[12] R. B. Buxton, L. R. Frank, E. C. Wong, B. Siewert, S. Warach, and R. R. Edelman, "A general kinetic model for quantitative perfusion imaging with arterial spin labeling," *Magn. Reson. Med.*, vol. 40, no. 3, pp. 383–396, 1998.

[13] D. J. J. Wang *et al.*, "The Value of Arterial Spin-Labeled Perfusion Imaging in Acute Ischemic Stroke – Comparison with Dynamic Susceptibility Contrast Enhanced MRI," *Stroke.*, vol. 43, no. 4, pp. 1018–1024, Apr. 2012.

[14] C. Chan, R. Fulton, R. Barnett, D. D. Feng, and S. Meikle, "Postreconstruction nonlocal means filtering of whole-body PET with an anatomical prior.," *IEEE Trans. Med. Imaging*, vol. 33, no. 3, pp. 636–650, Mar. 2014.